



Early Initiation of Inner Solar System Formation at the Dead-zone Inner Edge

Takahiro Ueda¹, Masahiro Ogihara^{1,2}, Eiichiro Kokubo¹, and Satoshi Okuzumi³¹National Astronomical Observatory of Japan, Osawa 2-21-1, Mitaka, Tokyo 181-8588, Japan; takahiro.ueda@nao.ac.jp²Earth-Life Science Institute, Tokyo Institute of Technology, Meguro-ku, Tokyo 152-8550, Japan³Department of Earth and Planetary Sciences, Tokyo Institute of Technology, Meguro, Tokyo 152-8551, Japan

Received 2021 July 13; revised 2021 September 29; accepted 2021 October 12; published 2021 October 27

Abstract

The inner solar system possesses a unique orbital structure in which there are no planets inside the Mercury orbit and the mass is concentrated around the Venus and Earth orbits. The origins of these features still remain unclear. We propose a novel concept that the building blocks of the inner solar system formed at the dead-zone inner edge in the early phase of the protosolar disk evolution, where the disk is effectively heated by the disk accretion. First, we compute the dust evolution in a gas disk with a dead zone and obtain the spatial distribution of rocky planetesimals. The disk is allowed to evolve both by a viscous diffusion and magnetically driven winds. We find that the rocky planetesimals are formed in concentrations around ~ 1 au with a total mass comparable to the mass of the current inner solar system in the early phase of the disk evolution within $\lesssim 0.1$ Myr. Based on the planetesimal distribution and the gas-disk structure, we subsequently perform N -body simulations of protoplanets to investigate the dynamical configuration of the planetary system. We find that the protoplanets can grow into planets without significant orbital migration because of the rapid clearing of the inner disk by the magnetically driven disk winds. Our model can explain the origins of the orbital structure of the inner solar system. Several other features such as the rocky composition can also be explained by the early formation of rocky planetesimals.

Unified Astronomy Thesaurus concepts: [Solar system formation \(1530\)](#); [Solar system terrestrial planets \(797\)](#); [Protoplanetary disks \(1300\)](#)

1. Introduction

The solar system is the most familiar planetary system and has been studied well for the past decades (e.g., Hayashi 1981; Chambers 2001; Raymond et al. 2009; Morishima et al. 2010; Jacobson & Morbidelli 2014; Lichtenberg et al. 2021). However, formation of the solar system is still the most interesting subject. The inner solar system possesses a unique dynamical configuration: large planets (Venus and Earth) sandwiched by two small planets (Mercury and Mars) and the absence of planets inside the orbit of Mercury. This configuration suggests that the building blocks of the inner solar system planets were not distributed uniformly but locally (Hansen 2009; Raymond et al. 2009). Hansen (2009) proposed a scenario that the inner solar system planets were formed from a narrow planetesimal annulus ranging from 0.7 to 1 au with a total mass of $2 M_{\oplus}$. This model can explain the configuration of the inner solar system planets.

Although several mechanisms have been proposed for the formation of a narrow annulus of rocky planetesimals (e.g., Drazkowska et al. 2016; Ogihara et al. 2018a), dust pileup at the dead-zone inner edge is one of the most preferred models for rocky planetesimal formation (e.g., Kretke et al. 2009; Chatterjee & Tan 2014; Ueda et al. 2019). At the dead-zone inner edge, the gas temperature reaches ~ 800 – 1000 K (e.g., Desch & Turner 2015; Jankovic et al. 2021), above which thermal ionization of the gas is sufficiently effective to activate magnetorotational instability (MRI; Gammie 1996). Across the dead-zone inner edge, the turbulent viscosity induced by the MRI steeply decreases from the inside out, resulting in a local maximum in the radial profile of the gas pressure (e.g., Dzyurkevich et al. 2010; Flock et al. 2017), which

traps solid particles (Whipple 1972; Adachi et al. 1976), and hence leads to the formation of rocky planetesimals by streaming instability (Youdin & Goodman 2005) and/or gravitational instability (Coradini et al. 1981).

Even if planetesimals form with the distribution proposed by Hansen (2009), their subsequent evolution depends on the evolution of the gas disk because protoplanets/planets interact with the gas disk gravitationally. One of the major difficulties is the so-called Type-I migration in which an Earth-sized planet at 1 au moves radially inward within a timescale of $\lesssim 1$ Myr (e.g., Ward 1997; Tanaka et al. 2002). Ogihara et al. (2015, 2018b) showed that Type-I migration can be suppressed and Earth-sized planets can survive at approximately 1 au if the magnetically driven disk winds dissipate the inner disk gas.

In this Letter, we propose a new concept that the formation of terrestrial planets starts at the dead-zone inner edge in the early phase of the disk evolution. The dead-zone inner edge is located at ~ 0.1 au for a typical passive T-Tauri disk (e.g., Ueda et al. 2017); however, it can be located beyond 1 au in the early phase of the disk evolution during which the accretion heating is effective. We demonstrate that rocky planetesimals can form around the current Earth orbit and grow into planets without significant orbital migration in the presence of the magnetically driven disk winds. Our calculation is divided into two parts. In Section 2, we show the setup and results of the dust-growth simulations. Subsequently, N -body simulations based on the obtained planetesimal distribution are presented in Section 3. The discussion and conclusions are presented in Sections 4 and 5, respectively.

2. From Dust to Planetesimals

In this section, we describe our dust-growth simulation method and subsequently present the time evolution of the protosolar disk as well as the obtained planetesimal distribution.

2.1. Simulation Setup: Dust and Gas-disk Evolution

We calculate dust evolution in a gas disk around a Sun-like star evolved with the magnetically driven disk winds as well as viscous diffusion. The method for the dust-growth simulation is the same as that used by Ueda et al. (2019). In this method, dust evolution in the gas disk is calculated based on a single-size approach, in which we trace the evolution of the maximum dust size in each radial grid (Sato et al. 2016). The dust grains are evolved by direct sticking, fragmentation, radial advection, and turbulent diffusion. The critical fragmentation velocities of silicate and icy grains are set as 3 and 10 m s⁻¹, respectively. The silicate and water-ice components are assumed to sublimate when the temperatures reach 150 and 1500 K, respectively. Just after the ice sublimation, silicate grains are assumed to have a size that is determined by the turbulence-induced fragmentation.

We employ a planetesimal formation algorithm described in Ueda et al. (2019; see also Drążkowska et al. 2016); if the midplane dust-to-gas mass ratio exceeds unity, dust is converted into planetesimals with a timescale of $\zeta^{-1}T_K$ where we adopt $\zeta = 10^{-4}$ as a fiducial.

We adopt the weak disk-wind model proposed by Suzuki & Ogihara (2016; see also Kunitomo et al. 2020; Taki et al. 2021) as the gas-disk model. We also implement the effect of a dead zone in the gas disk. MRI is assumed to occur if the disk midplane temperature is above $T_{\text{MRI}} = 800$ K or the gas surface density is below 20 g cm⁻². The former represents the effect of the thermal ionization of the disk gas and sets the dead-zone inner edge. The latter represents the effect of the nonthermal ionization induced by cosmic rays. The disk midplane is heated by the stellar irradiation and disk accretion. For the dust opacity, we adopt the opacity model given by Kunitomo et al. (2020), where the opacity is fixed to 4.5 cm² g⁻¹ for the rocky region. We adopt a turbulence strength of $\alpha_{\text{MRI}} = 2 \times 10^{-2}$ for the MRI-active region and $\alpha_{\text{DEAD}} = 2.3 \times 10^{-4}$ for the MRI-dead region as a fiducial model. As the initial condition, we assume a compact disk; the gas surface density follows a radial power-law index of 1.5 and an exponential tail with a cutoff radius of 15 au. The initial disk mass and the dust-to-gas mass ratio are set as $0.1M_{\odot}$ and 0.01, respectively.

2.2. Disk Evolution and Planetesimal Distribution

Figure 1 shows the time evolution of the gas surface density, dust surface density, and midplane temperature of the disk. In the beginning of the disk evolution, the gas surface density evolution is governed by the turbulent viscosity. The inner region of the disk is effectively heated by the disk accretion, and the dead-zone inner edge is located at $r \sim 4$ au, where r represents the radial distance from the star. Inside the dead-zone inner edge, the disk rapidly dissipates owing to the high viscosity, whereas the region outside the dead-zone inner edge is almost stationary until $t \sim 1$ Myr. The outermost region, $r \gtrsim 25$ au, also diffuses rapidly owing to the high viscosity because of the high ionization degree induced by the cosmic rays. As the gas surface density decreases, the midplane temperature also decreases, and hence the dead-zone inner edge moves inward with time. In the early phase ($t \lesssim 10^5$ yr), the gas surface density at ~ 0.2 –4 au is shaped by the migrating dead-zone inner edge. Since the dead-zone inner edge migrates, the gas surface density gradient is shallower than that obtained from a quasi-static model (e.g., Ueda et al. 2019). At $t \sim 10$ kyr, rocky grains start to pile up at ~ 2 au. With the given

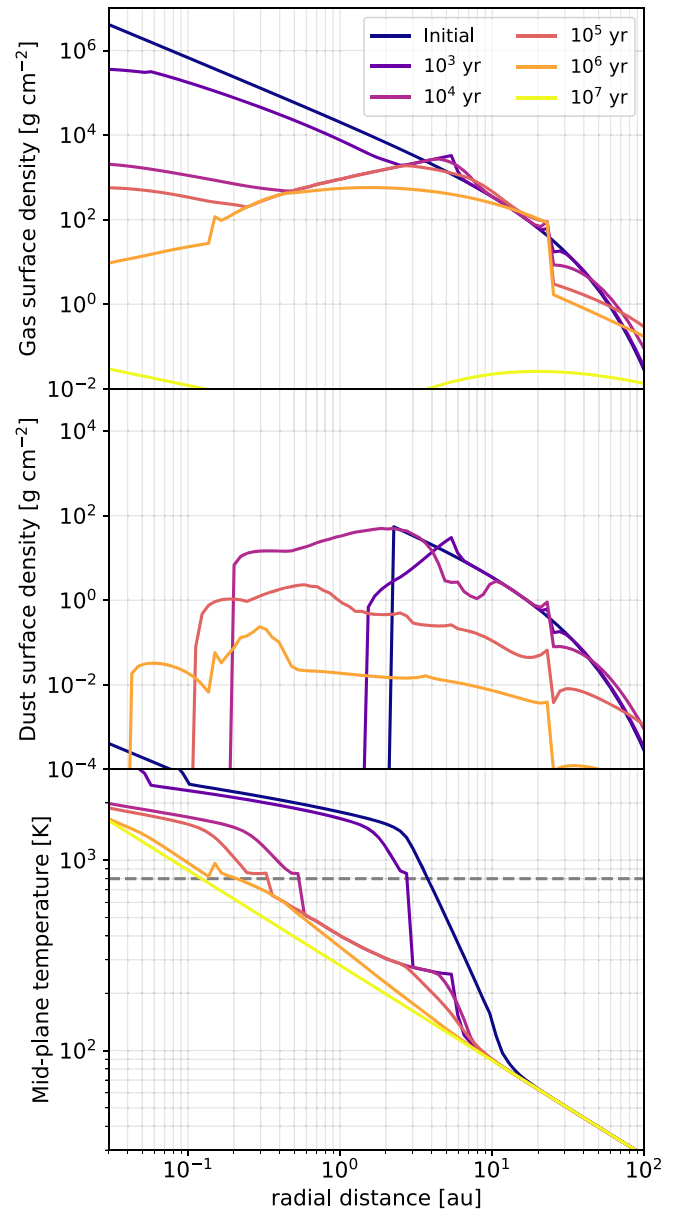


Figure 1. Time evolution of gas surface density (top), dust surface density (middle), and midplane temperature (bottom).

turbulence strength ($\alpha_{\text{DEAD}} = 2.3 \times 10^{-4}$), rocky grains do not pile up strongly; however, they accumulate marginally just outside the dead-zone inner edge. Following the radial motion of the dead-zone inner edge, dust accumulation also moves inward: ~ 2 , 0.7, and 0.3 au at 10^4 , 10^5 , and 10^6 yr, respectively.

Figure 2 shows the planetesimal distribution obtained from the simulation of the dust evolution.

For reference, we also show the results with $\alpha_{\text{DEAD}} = 2.1 \times 10^{-4}$ and 2.5×10^{-4} . We clearly see that rocky planetesimals form around the solar system terrestrial planet region. For $\alpha_{\text{DEAD}} = 2.3 \times 10^{-4}$, the surface density profile of the formed planetesimals is comparable to that proposed by Hansen (2009). The inner edge of the planetesimal belt is at $r \simeq 0.6$ au, and no planetesimals form inside it. If the turbulence is stronger ($\alpha_{\text{DEAD}} = 2.5 \times 10^{-4}$), the dust pileup is suppressed because of the stronger turbulent mixing, and hence the total mass of the planetesimals is smaller. In contrast, if the turbulence is weaker ($\alpha_{\text{DEAD}} = 2.1 \times 10^{-4}$), rocky

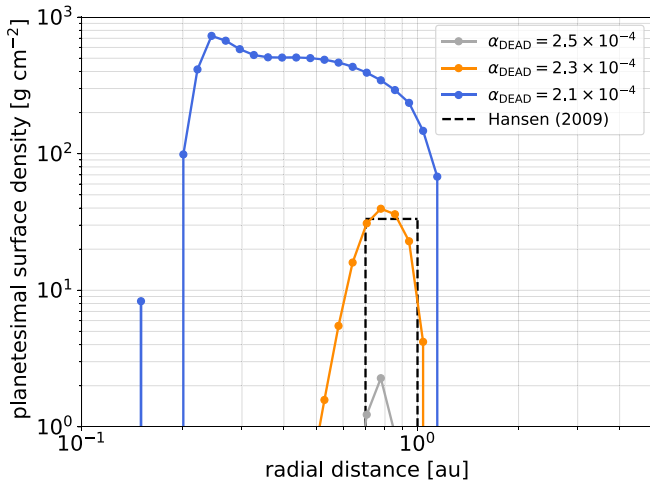


Figure 2. Obtained planetesimal surface density profile with $\alpha_{\text{DEAD}} = 2.3 \times 10^{-4}$ (orange). The black dashed line corresponds to the planetesimal distribution proposed by Hansen (2009). For reference, results of simulations with $\alpha_{\text{DEAD}} = 2.1 \times 10^{-4}$ (blue) and 2.5×10^{-4} (gray) are also shown.

grains pile up efficiently, and hence a significant amount of planetesimals form.

The outer edge of the planetesimal belt is determined by the location of the dead-zone inner edge when the pileup starts. In our model, the disk is initially massive and compact (mass of $0.1M_{\odot}$ and radius of 15 au), and hence the dead zone can be located beyond 1 au. The inner edge of the planetesimal belt is determined by the balance between the radial mass flux of the drifting pebbles and the turbulent mixing. Because the dust mass flux is a decreasing function of time (Lambrechts & Johansen 2014), the turbulent mixing dominates the accumulation of dust at some point. Because we select the turbulence strength to be such that the dust pileup is marginal ($\alpha_{\text{DEAD}} = 2.3 \times 10^{-4}$), the planetesimals concentrate at $r \sim 0.6\text{--}1$ au, which is preferable for the formation of solar system terrestrial planets. If the turbulence strength is sufficiently weak, planetesimals continuously form at the moving dead-zone inner edge, and the planetesimal belt reaches $r \sim 0.1$ au. This broad and massive planetesimal belt will be unsuitable for the inner solar system; however, it will be preferable for the formation of close-in super-Earth systems.

The strong dependence of the planetesimal distribution on the turbulence strength indicates that there are two regimes in the planet formation at the dead-zone inner edge. In the weak turbulence regime ($\alpha_{\text{DEAD}} \lesssim 2.1 \times 10^{-4}$), rocky planetesimals efficiently form in the inner region of the disk, which can account for super-Earth systems. In the strong turbulence regime ($\alpha_{\text{DEAD}} \gtrsim 2.5 \times 10^{-4}$), no planetesimals/planets form in the inner region of the disk. The inner solar system lies in between these two regimes.

2.3. Parameter Dependence

So far, we focus on our fiducial model, which is the best for inner solar system formation in our calculations. However, it is worth describing the parameter dependence on the planetesimal distribution. Table 1 summarizes parameters and planetesimal distribution (total mass M_{plts} and peak position in planetesimal surface density r_{peak}) at $t = 10^5$ yr obtained in different models.

The total planetesimal mass is also sensitive to the critical fragmentation velocity v_f . If $v_f = 1 \text{ m s}^{-1}$, no planetesimals form,

Table 1
Parameter Dependence on Planetesimal Distribution

ID	α_{DEAD}	v_f (m s^{-1})	r_d (au)	ζ	M_{plts} (M_{\oplus})	r_{peak} (au)
0	2.3×10^{-4}	3	15	10^{-4}	2.2	0.78
1	2.1×10^{-4}	3	15	10^{-4}	48	0.24
2	2.5×10^{-4}	3	15	10^{-4}	0.06	0.78
3	3.0×10^{-4}	3	15	10^{-4}	0	N/A
4	2.3×10^{-4}	1	15	10^{-4}	0	N/A
5	2.3×10^{-4}	10	15	10^{-4}	78	0.64
6	2.3×10^{-4}	3	30	10^{-4}	2.8	0.71
7	2.3×10^{-4}	3	100	10^{-4}	13.8	0.53
8	2.3×10^{-4}	3	15	10^{-3}	6.7	0.78
9	2.3×10^{-4}	3	15	10^{-5}	0.28	0.78

while planetesimals with a total mass of $78M_{\oplus}$ form when $v_f = 10 \text{ m s}^{-1}$, in our model. This is because lower v_f makes dust smaller, leading to inefficient dust trapping. The total planetesimal mass is an increasing function of the planetesimal formation efficiency ζ ; $M_{\text{plts}} = 0.28, 2.2,$ and $6.7M_{\oplus}$ for $\zeta = 10^{-5}, 10^{-4},$ and 10^{-3} . It is worth emphasizing that the total planetesimal mass can decrease (increase) to $2M_{\oplus}$ even with $\zeta = 10^{-3}$ by slightly increasing (decreasing) α_{DEAD} . On the other hand, the location where planetesimals form is mainly determined by the gas surface density and hence the disk size for a given disk mass ($0.1M_{\odot}$ in our model). The gas disk needs to have a initial radius of <30 au to form a narrow planetesimal belt at a current terrestrial planet region.

3. From Protoplanets to Planets

In this section, we perform N -body simulations of planet formation to investigate the subsequent evolution of formed planetesimals.

3.1. Simulation Setup: N -body Simulations

As the initial condition, protoplanets with masses of $0.01 M_{\oplus}$ and eccentricities/inclinations of $\simeq 0.01$ are distributed with a surface density profile that is the same as the planetesimal distribution presented in Section 2. We use the gas-disk structure shown in Figure 1 and start N -body simulations at a time of 30 kyr. Although not discussed in this Letter, additional simulations are performed in which N -body simulations are initiated at a time of 1 Myr with the same distribution of protoplanets with our fiducial model, which reflects the time elapse for planetesimals to grow into protoplanets. We confirmed that this does not influence our conclusions. In the calculation, we compute the gravitational interaction between protoplanets orbiting around the Sun and assume a perfect accretion when they collide. We also consider planet–disk interaction.

3.2. Evolution of Protoplanets

Figure 3 shows the time evolution of the semimajor axes of the protoplanets. The protoplanets collide with each other and eventually form four planets with masses greater than the Mercury mass at 200 Myr after the formation of protoplanets. Although the turbulent viscosity dominates the early disk evolution, the magnetically driven disk winds clear the disk gas

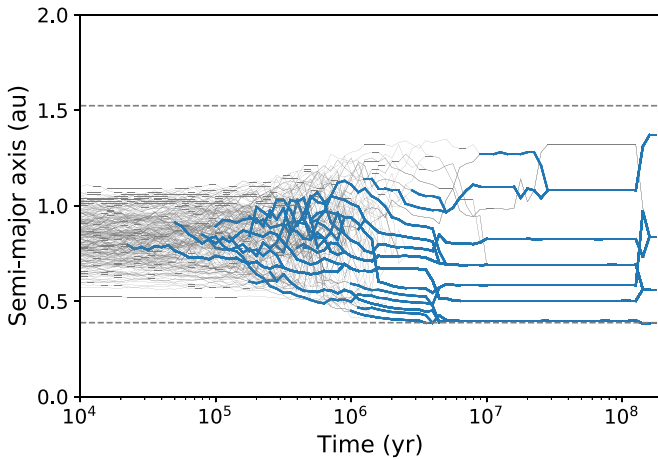


Figure 3. Time evolution of semimajor axis. Dashed lines indicate semimajor axes of Mercury and Mars. Planets with masses greater than Mercury mass are indicated by thick lines.

efficiently in the later phase ($\gtrsim 10^6$ yr). Owing to the inner-disk clearing by the magnetically driven disk winds, the inner disk becomes flatter and finally dissipates within 10^7 yr (Figure 1). This flat (or even positive) density profile induces a positive corotation torque on the protoplanets, and hence even massive protoplanets of masses similar to Earth mass do not significantly migrate (see the Appendix).

Here we summarize our model in Figure 4. In the early phase of the disk evolution, the dead-zone inner edge is located beyond 1 au owing to the efficient accretion heating. Rocky planetesimals form in the terrestrial planet region by the dust pileup at the dead-zone inner edge within 0.1 Myr. The total mass of the rocky planetesimals is sensitive to the turbulence strength. When $\alpha_{\text{DEAD}} = 2.3 \times 10^{-4}$, rocky planetesimals with a total mass of $\sim 2M_{\oplus}$ form in a narrow annulus at 1 au, which is preferable for the formation of inner solar system planets. The formed planetesimals can grow into planets without significant migration because the inner disk rapidly dissipates by the magnetically driven disk winds.

4. Discussions

4.1. Features of the Inner Solar System

It is noteworthy that our model can reproduce various characteristics of the inner solar system. Figure 5 summarizes 10 runs of N -body simulations that start with different initial locations of the protoplanets. The important feature that no planets form within the orbit of Mercury was reproduced. Regarding the mass distribution, the innermost and outermost planets are less massive, which is consistent with the low masses of Mercury and Mars.

Our model also has important implications for planetary composition. The water snow line can be located within 1 au during disk evolution (Oka et al. 2011). If terrestrial planets form during this phase, they might be enriched by water. To prevent icy materials (i.e., pebbles and planetesimals) from growing near 1 au, the gas disk around the snow line should be dry (Morbidelli et al. 2016). However, our model proposes that rocky planetesimals form before the snow line moves in; therefore, there is no need to assume a dry disk gas during the formation of planetesimals.

As a different problem, there is a possibility that icy pebbles form in the outer region and experience a radial drift to ~ 1 au, making the terrestrial planets water-rich. The radial drift of icy

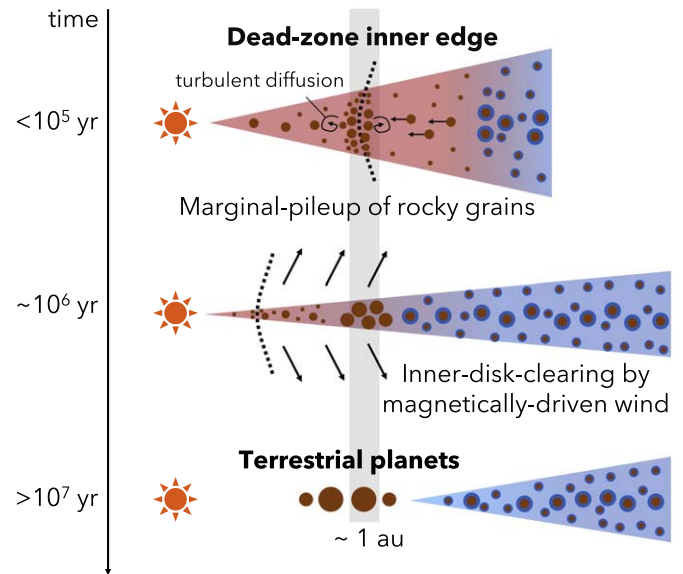


Figure 4. Schematic of terrestrial planet formation starting at the dead-zone inner edge.

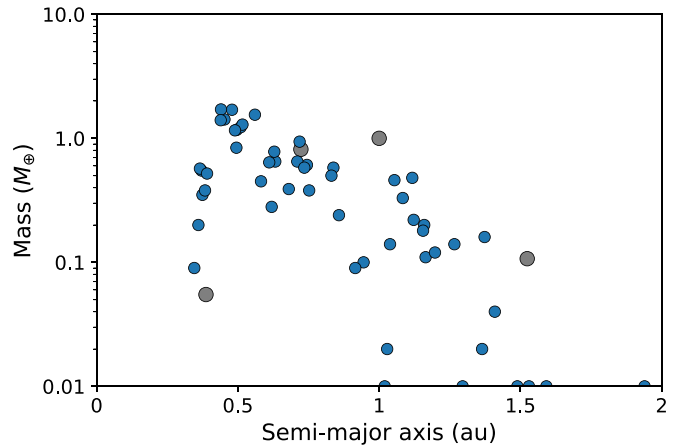


Figure 5. Comparison of mass distributions obtained from 10 runs of our simulations (blue) and solar system terrestrial planets (red).

pebbles can be hindered by the formation of a proto-Jupiter (Morbidelli et al. 2016; Kruijer et al. 2017). A potential mechanism forming a Jupiter core is icy planetesimal formation immediately behind the water snow line (e.g., Drążkowska & Alibert 2017; Drążkowska & Dullemond 2018; Hyodo et al. 2019). Therefore, we expect that a proto-Jupiter was formed at the water snow line immediately after the terrestrial planets form at the dead-zone inner edge.

Other features of the terrestrial planets in the solar system can also be reproduced. The angular momentum deficit (Laskar 1997), which represents the magnitude of the eccentricity and inclination, is as small as $\sim 10^{-3}$, which is consistent with that of the current inner solar system. In addition, the last giant impacts experienced by massive terrestrial planets with masses of $\simeq 1M_{\oplus}$ are also consistent with the timing of the moon-forming impact of 50–150 Myr (e.g., Kleine et al. 2009).

4.2. Importance of Early Phase Disk Evolution

We demonstrated that inner solar system analogs can form under a specific disk condition. As shown in Section 2.3, the

planetesimal distribution is sensitive to disk parameters. Particularly, the total mass of planetesimals is very sensitive to the turbulence strength in the dead zone. Although we fix α_{DEAD} , it would vary with time because of fluctuations in the gas motion and of different mechanisms that generate the turbulence. The small variation in the turbulence strength might affect the total mass of planetesimals. To fully understand the formation of planetesimals via the dust pileup, detailed (magneto)hydrodynamical simulations combined with the dust evolution would be necessary.

The initial disk size is also important particularly for the radial position of planets. The initial disk parameters strongly depend on the disk formation processes and parent cloud properties, such as an angular momentum of the collapsing core (e.g., Hueso & Guillot 2005). To form a compact disk with a radius of ~ 15 au, the angular velocity of the molecular cloud core needs to be $\sim 5 \times 10^{-15} \text{ s}^{-1}$, which is comparable to the typical observed value (Goodman et al. 1993). In this study, we do not consider the disk formation phase and assume a power-law disk as an initial condition. However, the dust grains grow and potentially form planetesimals even in the disk formation phase (Drażkowska & Dullemond 2018). The detailed parameter study considering the disk formation phase would be important for understanding the diversity of exoplanets and will be performed in the near future.

The evolution of the global magnetic field is also crucial for both disk formation and evolution. Our model requires inner-disk clearing by the magnetically driven disk winds, which depend on the strength of the large-scale magnetic field threading the disk (e.g., Bai 2016). In addition, the wind-driven accretion can suppress the midplane heating because heat energy is released at the upper layer (Mori et al. 2019). However, we expect that the location of the dead-zone inner edge would not be affected by the non-ideal magnetohydrodynamical effect because it takes place only outside the dead-zone inner edge.

It is worth noting that recent Atacama Large Millimeter/submillimeter Array (ALMA) observations have shown that young protoplanetary disks have substructures in dust emission (e.g., Sheehan & Eisner 2018; Nakatani et al. 2020; Segura-Cox et al. 2020). The prevalence of substructures suggests that local dust trapping occurs and planetesimals might form within them in the early phase of the disk evolution. Although most of the observed substructures are in the outer region ($\gtrsim 10$ au), it is still unclear if the inner disk also has substructures. Observations of the terrestrial planet regions are still difficult with current observing facilities, such as ALMA, because we require $< 0''.01$ resolution and observing wavelengths where the disk is optically thin. Future subcentimeter observations with such as the next-generation Very Large Array will provide insights on terrestrial planets formation.

4.3. Comparison to Other Models with the Dead-zone Inner Edge

In this work we demonstrated that the inner solar system analogs form at the dead-zone inner edge if the disk is initially compact and the turbulence in the dead zone can keep balance between dust accumulation and diffusion. In contrast, most of the previous studies focus on the dead-zone inner edge as a formation site of close-in planets (e.g., Chatterjee & Tan 2014; Hu et al. 2018; Jankovic et al. 2019). One of the biggest differences between ours and the previous models is the disk

surface density. In our model we consider a compact and massive disk where the gas surface density is high enough to heat the midplane at 1 au above > 800 K, while previous studies have used less massive disks. It would be natural to focus on the compact disk because dust at 1 au is expected to grow within a timescale of ~ 100 yr and protoplanetary disks are expected to be more compact in earlier phase.

Furthermore, the previous studies mostly consider the regime where dust particles are easily trapped at the dead-zone inner edge. However, dust particles are not necessarily trapped even if the radial gas pressure profile has a pressure maximum because turbulent diffusion prevents it (Ueda et al. 2019). Our work showed that the marginal dust trapping at the dead-zone inner edge accounts for the inner solar system, not close-in super-Earths. Since the inner solar system analogs form only with a tight parameter space, the inner solar system might be rare compared to super-Earth systems.

5. Conclusions

In the early stage of disk evolution, owing to the high surface density, the gas-disk accretion heats the disk midplane, and the dead-zone inner edge is located beyond 1 au. As the disk evolves, the surface density decreases and the dead-zone inner edge moves inward. With the inward migration of the dead-zone inner edge, dust particles pile up at the dead-zone inner edge and planetesimals form. We found that under specific conditions—initial disk mass of $0.1 M_{\odot}$, initial disk radius of 15 au, and turbulence strength in the dead zone of 2.3×10^{-4} —rocky planetesimals with a total mass of $\sim 2 M_{\oplus}$ can form in the current terrestrial planet region, with no planetesimals inside $r \simeq 0.6$ au within 0.1 Myr. There are two regimes in planetesimal formation at the dead-zone inner edge: no rocky planetesimals form due to efficient turbulence mixing ($\alpha_{\text{DEAD}} > 2.3 \times 10^{-4}$) and a significant amount of rocky planetesimals form by efficient dust trapping ($\alpha_{\text{DEAD}} < 2.3 \times 10^{-4}$). The inner solar system lies in between these two regimes. We also found that protoplanets can grow into planets without significant migration in the disk structure because the magnetically driven disk winds rapidly dissipate the inner disk gas and suppress Type-I migration. Based on these results, we propose a hypothesis that the solar system terrestrial planets formed by dust trapping at the dead-zone inner edge. This model can explain the origins of various features of the terrestrial planets in the solar system including the mass and semimajor axis distribution and the rocky composition.

We thank Masanobu Kunitomo for useful comments. T.U. is supported by JSPS KAKENHI grant No. JP19J01929. M.O. is supported by JSPS KAKENHI grant Nos. 18K13608 and 19H05087. E.K. and S.O. are supported by JSPS KAKENHI grant No. 18H05438. Numerical computations were in part carried out on PC cluster at Center for Computational Astrophysics of the National Astronomical Observatory of Japan.

Appendix

Effect of Corotation Torque on Suppression of Migration

It is known that planets with masses larger than the Mars mass undergo rapid inward migration. Therefore, even if protoplanets form in a narrow annulus at ~ 1 au, they are caused to penetrate the inner region by the subsequent migration. Note that the disk–planet interaction was not considered in Hansen (2009). In Section 3.2, we showed that Type-I migration of planets is

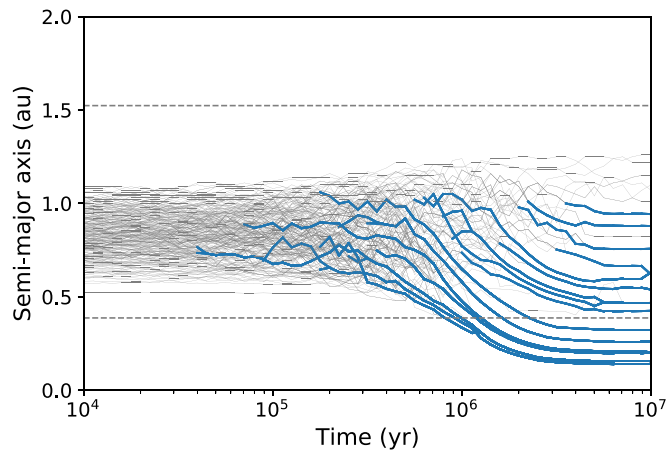

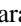

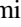


Figure 6. Same as Figure 3, but without the effects of the corotation torque.

significantly suppressed and no planets migrate inside the orbit of Mercury. This is partly because the gas surface density in the inner region is reduced by the disk winds. In addition, the slope of the gas surface density is changed by the disk winds, which also plays an important role in suppressing the inward migration. Here, we see the effect of the positive corotation torque due to the change in the gas surface density profiles. Figure 6 shows the result of a simulation in which the effect of the corotation torque is artificially ignored. Comparing the results of the simulations shown in Figures 3 and 6, an inward migration of the planets are clearly visible in Figure 6. Consequently, the planets move inside the orbit of Mercury. This result confirms that the change in the surface density profile is important for the suppression of Type-I migration.

ORCID iDs

Takahiro Ueda  <https://orcid.org/0000-0003-4902-222X>
 Masahiro Ogihara  <https://orcid.org/0000-0002-8300-7990>
 Eiichiro Kokubo  <https://orcid.org/0000-0002-5486-7828>
 Satoshi Okuzumi  <https://orcid.org/0000-0002-1886-0880>

References

Adachi, I., Hayashi, C., & Nakazawa, K. 1976, *PThPh*, 56, 1756
 Bai, X.-N. 2016, *ApJ*, 821, 80
 Chambers, J. E. 2001, *Icar*, 152, 205
 Chatterjee, S., & Tan, J. C. 2014, *ApJ*, 780, 53

Coradini, A., Magni, G., & Federico, C. 1981, *A&A*, 98, 173
 Desch, S. J., & Turner, N. J. 2015, *ApJ*, 811, 156
 Drażkowska, J., & Alibert, Y. 2017, *A&A*, 608, A92
 Drażkowska, J., Alibert, Y., Moore, B., et al. 2016, *A&A*, 594, A105
 Drażkowska, J., & Dullemond, C. P. 2018, *A&A*, 614, A62
 Dzyurkevich, N., Flock, M., Turner, N. J., Klahr, H., & Henning, T. 2010, *A&A*, 515, A70
 Flock, M., Fromang, S., Turner, N. J., & Benisty, M. 2017, *ApJ*, 835, 230
 Gammie, C. F. 1996, *ApJ*, 462, 725
 Goodman, A. A., Benson, P. J., Fuller, G. A., & Myers, P. C. 1993, *ApJ*, 406, 528
 Hansen, B. M. S. 2009, *ApJ*, 703, 1131
 Hayashi, C. 1981, *PThPS*, 70, 35
 Hu, X., Tan, J. C., Zhu, Z., et al. 2018, *ApJ*, 857, 20
 Hueso, R., & Guillot, T. 2005, *A&A*, 442, 703
 Hyodo, R., Ida, S., & Charnoz, S. 2019, *A&A*, 629, A90
 Jacobson, S. A., & Morbidelli, A. 2014, *RSPTA*, 372, 0174
 Jankovic, M. R., Owen, J. E., & Mohanty, S. 2019, *MNRAS*, 484, 2296
 Jankovic, M. R., Owen, J. E., Mohanty, S., & Tan, J. C. 2021, *MNRAS*, 504, 280
 Kleine, T., Touboul, M., Bourdon, B., et al. 2009, *GeoCoA*, 73, 5150
 Kretke, K. A., Lin, D. N. C., Garaud, P., & Turner, N. J. 2009, *ApJ*, 690, 407
 Kruijer, T. S., Burkhardt, C., Budde, G., & Kleine, T. 2017, *PNAS*, 114, 6712
 Kunitomo, M., Suzuki, T. K., Inutsuka, S. I., et al. 2020, *MNRAS*, 492, 3849
 Lambrechts, M., & Johansen, A. 2014, *A&A*, 572, A107
 Laskar, J. 1997, *A&A*, 317, L75
 Lichtenberg, T., Drażkowska, J., Schönbachler, M., Golabek, G. J., & Hands, T. O. 2021, *Sci*, 371, 365
 Morbidelli, A., Bitsch, B., Crida, A., et al. 2016, *Icar*, 267, 368
 Mori, S., Bai, X.-N., & Okuzumi, S. 2019, *ApJ*, 872, 98
 Morishima, R., Stadel, J., & Moore, B. 2010, *Icar*, 207, 517
 Nakatani, R., Liu, H. B., Ohashi, S., et al. 2020, *ApJL*, 895, L2
 Ogihara, M., Kobayashi, H., Kobayashi, S.-I., & Kobayashi, T. K. 2015, *A&A*, 579, A65
 Ogihara, M., Kokubo, E., Suzuki, T. K., & Morbidelli, A. 2018a, *A&A*, 612, L5
 Ogihara, M., Kokubo, E., Suzuki, T. K., & Morbidelli, A. 2018b, *A&A*, 615, A63
 Oka, A., Nakamoto, T., & Ida, S. 2011, *ApJ*, 738, 141
 Raymond, S. N., O'Brien, D. P., Morbidelli, A., & Kaib, N. A. 2009, *Icar*, 203, 644
 Sato, T., Okuzumi, S., & Ida, S. 2016, *A&A*, 589, A15
 Segura-Cox, D. M., Schmiedeke, A., Pineda, J. E., et al. 2020, *Natur*, 586, 228
 Sheehan, P. D., & Eisner, J. A. 2018, *ApJ*, 857, 18
 Suzuki, T. K., Ogihara, M., Morbidelli, A. R., Crida, A., & Guillot, T. 2016, *A&A*, 596, A74
 Taki, T., Kuwabara, K., Kobayashi, H., & Suzuki, T. K. 2021, *ApJ*, 909, 75
 Tanaka, H., Takeuchi, T., & Ward, W. R. 2002, *ApJ*, 565, 1257
 Ueda, T., Flock, M., & Okuzumi, S. 2019, *ApJ*, 871, 10
 Ueda, T., Okuzumi, S., & Flock, M. 2017, *ApJ*, 843, 49
 Ward, W. R. 1997, *Icar*, 126, 261
 Whipple, F. L. 1972, in Proc. of 21st Nobel Symp., From Plasma to Planet, ed. A. Elvius (New York: Wiley), 211
 Youdin, A. N., & Goodman, J. 2005, *ApJ*, 620, 459